Secretome-Mediated Neuroprotective Effects of the hiPSC-derived Glial and Neuronal Progenitor Cells in the Hypoxia-Induced Neuronal Damage (Comparative Study)

Diana Salikhova
Research centre for medical genetics, Research institute of Human Morphology
Tatiana Bukharova
Research centre for medical genetics
Elvira Cherkashova
FSBI Federal center of brain research and neurotechnologies of FMBA
Daria Namestnikova
Pirogov Russian National Research Medical University
Georgy Leonov
Research centre for medical genetics
Maria Nikitina
Research Institute of Human Morphology
Ilya Gubskiy
FSBI Federal center of brain research and neurotechnologies of FMBA
Gevorg Akopyan
FSBI Federal center of brain research and neurotechnologies of FMBA
Andrey Elchaninov
Research Institute of Human Morphology
Konstantin Midiber
Research institute of Human Morphology
Natalia Bulatenco
Research centre for medical genetics
Victoria Mokrousova
Research centre for medical genetics
Andrey Makarov
Research Institute of Human Morphology
Konstantin Yarygin
Institute of Biomedical Chemistry, Russian Medical Academy of Continuous Proffesional Education
Vladimir Chekhonin
Pirogov Russion National Research Medical University

Liudmila Mikhaleva
Research Institute of Human Morphology
Timur Fatkhudinov (tfat@yandex.ru)
Research Center for Obstetrics, Gynecology and Perinatology of Ministry of Healthcare of the Russian Federation https://orcid.org/0000-0002-6498-5764
Dmitry Goldshtein
Research centre for medical genetics, RUDN University

Research

Keywords: neuronal progenitor cells, glial progenitor cells, conditioned media, middle cerebral artery occlusion, experimental ischemic stroke, hypoxia, induced pluripotent stem cells, proteome, secretome, neuroprotection, nervous tissue repair

Posted Date: February 3rd, 2021

DOI: https://doi.org/10.21203/rs.3.rs-49227/v2

Abstract

Background: Stem cell secretomes hold great promise for regenerative medicine. This study is focused on the secretome-mediated neuroprotective effects of the human induced pluripotent stem cell-derived neuronal and glial progenitor cells. Therapeutic properties of the secretomes were assessed under conditions of the hypoxia-induced neuronal damage *in vitro* and *in vivo*.

Methods: Secretory activity of the cultured neuronal and glial progenitor cells was analyzed by proteomic and immunosorbent-based approaches. Conditioned media collected from the cultures was tested for neuroprotective properties *in vitro* and *in vivo*.

In vitro experiments involved exposure of SH-SY5Y cells to the conditioned media during the recovery from the cobalt chloride-induced hypoxia. Neuroprotective effects were assessed by cell survival and neurite outgrowth. Cell survival indicators included MTT and LDH tests, vital staining with propidium iodide and Hoechst 33342, and polymerase chain reaction assay for the expression of apoptosis-related genes. Neurite outgrowth was assessed by alterations in SH-SY5Y cell morphology and *MAP2*/*GAP43* gene expression dynamics.

In vivo experiments involved intra-arterial administration of the conditioned media to laboratory rats during the recovery from experimental ischemic stroke. Neuroprotective effects were assessed by overall survival, neurologic deficit and infarct volume dynamics, as well as by the end-point values of the apoptosis- and inflammation-related gene expression levels, the extent of microglia/macrophage infiltration, and the numbers of newly formed blood vessels in the affected area of the brain.

Results: Secretomes of glial and neuronal progenitor cells partially overlapped, with specific proteins (found in secretome of one of the studied cultures and absent from the other) constituting, respectively, 31% and 45%. The glial progenitor cell-conditioned media showed higher content of neurotrophins (BDNF, GDNF, CNTF and NGF).

Moreover, the glial progenitor cell-conditioned media was superior to the neuronal progenitor cell-conditioned media in facilitating neurite outgrowth and increasing SHSY-5Y cell survival after the cobalt dichloride-induced hypoxia. In addition, intra-arterial infusion of the glial progenitor cell-conditioned media to the animals after experimental ischemic stroke significantly enhanced functional recovery and promoted tissue repair at the site of brain damage, as indicated by reduced microglia/macrophage infiltration, decreased expression of pro-apoptotic gene *Bax* and pro-inflammatory cytokine gene *Tnf*, increased expression of anti-inflammatory cytokine genes (*Il4*, *Il10*, *Il13*), and increased numbers of newly formed blood vessels within the damaged area. None of these effects were exerted by the neuronal progenitor cell-conditioned media.

Conclusions: The results indicate pronounced cytoprotective, anti-inflammatory and angionenic properties of soluble factors secreted by glial progenitor cells.

Introduction

Deterioration of brain function in ischemic stroke is overwhelming. The acute hypoxic damage to brain tissue causes focal and generalized neuronal death with diverse neurological sequelae [1]. Effectiveness of treatment and rehabilitation of the patients after acute cerebrovascular episodes remains extremely low. In the absence of etiological treatment, it is important to promote rehabilitation of the patients by stimulating nervous tissue repair [2]. New efficient maintenance therapies for cerebrovascular diseases are highly relevant.

Stem cells represent a promising and rapidly developing tool of regenerative medicine. The efficiency of cell therapies is based on two fundamental properties of the transplant — its ability to replace the destroyed differentiated cells of the tissue (replacement mechanism) and its ability to secrete regulatory molecules for the processes of inflammation, angiogenesis and regeneration (paracrine mechanism) [3,4].

The paracrine concept of cell therapies is currently taking the lead [5,6]. Accordingly, the conditioned tissue culture media become of increasing interest as a source of biologically active molecules. Neurotrophins, cytokines and other regulatory molecules which accumulate in the tissue culture media can exert complex positive effects in various pathological conditions [4]. Good prospects for the use of stem cell-conditioned media for the treatment of neurodegenerative and vascular diseases was demonstrated in a number of studies [7–9].

Neuronal and glial progenitor cells (respectively, NPCs and GPCs) can be derived from human induced pluripotent stem cells (hiPSCs). Positive influence of their secretomes on the damaged nervous tissue appears plausible. This influence has not yet been studied and no substantive information on this subject can be found in the literature.

Here we report the results of comparative assessment of neuroprotective paracrine effects of the hiPSC-derived NPCs and GPCs. Therapeutic relevance of the NPC- and GPC-conditioned media was assessed *in vitro* and *in vivo* by using, respectively, SH-SY5Y model of cobalt-induced hypoxia and rat experimental model of ischemic stroke.

Materials And Methods

Cell culture and conditioned media preparation

hiPSCs were derived from human dermal fibroblasts by using CTS CytoTune-iPS 2.1 Sendai Reprogramming Kit (Invitrogen, USA). To obtain neural stem cells (NSCs) for subsequent differentiation into neuronal and glial lineages, hiPSCs were cultured in DMEM/F12 (Gibco, USA) supplemented with N-2 (to 1X, Gibco), 2 mM L-glutamine (PanEco, Russia), 100 mg/L penicillin-streptomycin (PanEco), 10 μM SB431542 (Stemcell Technologies, USA), 2 μM dorsomorphin (Stemcell Technologies) and 200 nM LDN193189 (Sigma-Aldrich, USA) [10].

To obtain NPCs, NSCs were cultured for 2 weeks in DMEM/F12 (PanEco) supplemented with B-27 (to 1X, Gibco), 2 mM L-glutamine, 100 mg/L penicillin-streptomycin, 10 ng/mL FGF-2 (ProSpec, UK) and 1 μM purmorphamine (Stemcell Technologies) [11].

To obtain GPCs, NSCs were cultured in DMEM/F12-based growth medium supplemented invariably with N-2, 2 mM L-glutamine, 100 mg/L penicillin-streptomycin and 1% fetal bovine serum (PanEco). The induction proceeded in 3 stages, 3 days each. For the first stage, the growth medium was additionally supplemented with 10 ng/mL FGF-2 and 20 ng/mL EGF (ProSpec). For the second stage, the growth medium was additionally supplemented with 10 ng/mL FGF-2, 20 ng/mL EGF, and 20 ng/mL CNTF (PeproTech, USA). For the third stage, the growth medium was additionally supplemented with 20 ng/mL EGF and 20 ng/mL CNTF [12,13].

To obtain the conditioned media (CM), NPC and GPC cultures were washed twice with PBS and incubated in DMEM/F12 (PanEco) for 12 h. The medium was collected and centrifuged for 5 min at 3000 rpm. The supernatant was passed through 0.2 μm syringe filter (PanEco) and used in the experiments.

Immunocytochemistry

The cells were fixed in 4% paraformaldehyde solution (PanEco) for 10 min at room temperature, washed with PBS, pre-incubated in 0.25% Triton X-100 and 1% BSA in PBS for 30 min, and further incubated with primary antibodies to βIII tubulin (ab182070, Abcam, UK), S100b (ab52642, Abcam), NANOG, SSEA4, OCT4, TRA-1-81, SOX2 (StemLight Pluripotency Antibody Kit, Cell Signaling Technology, USA), pancytokeratin (ab7753, Abcam), desmin (ab32362, Abcam), α-fetoprotein (ab3980, Abcam), Nestin (ab105389, Abcam) or PAX6 (ab5790, Abcam) at +4 °C overnight. Secondary antibodies (Alexa Fluor 555 or Alexa Fluor 488 conjugated, Invitrogen) were applied for 60 min in the dark. The nuclei were counterstained with DAPI solution (1 μg/mL in PBS). The signals were observed and images recorded with an Axio Observer.D1 inverted fluorescence microscope equipped with AxioCam HRc (Carl Zeiss, Germany).

Flow cytometry

The cells were detached with Versene solution (PanEco) and pelleted by centrifugation at 1800 rpm for 5 min, then washed with HBSS (PanEco), fixed in 4% paraformaldehyde for 10 min, washed with PBS, permeabilized with 70% methanol on ice for 10 min, washed twice with PBS and collected by centrifugation at 1800 rpm for 5 min. Fixed cells were incubated with primary antibodies to PAX6 (ab5790, Abcam), glial marker S100b (ab52642, Abcam) or neuronal marker βIII tubulin (ab182070, Abcam) at +4 °C for 12 h, then washed with PBS, collected by centrifugation at 1800 rpm for 5 min and incubated with secondary antibodies (Alexa Fluor 488 conjugated, Invitrogen) for 60 min in the dark. Fixed cells exposed to secondary antibodies only were used as a negative control for the flow cytometry-based quantification. Stained cells were analyzed on a CyFlow ML flow cytometer with FloMax software (Partec, Germany).

Proteomic analysis

Ultimate 3000 RSLCnano HPLC system (Thermo Scientific, USA) connected to Q-exactive HF mass spectrometer (Thermo Scientific) was used for the analysis. Mass spectra were recorded in the ion-positive mode with nanoelectrospray ionization. Identification of proteins in the spectra was carried out in SearchGUI v.3.3.16 software with X!Tandem, OMSSA and MS-GF+ algorithms (Vaudel M. et al., 2011). The alignments were made with Uniprot database ('human'-filtered). Structuring of the data by classes and functions of the proteins was carried out by using Uniprot and PANTHER databases [15].

Enzyme-linked immunosorbent assay (ELISA)

Concentrations of GDNF, BDNF, NGF and CNTF in CM were measured by ELISA (RnD systems, USA) in accordance with the manufacturer's protocol. The collected CM samples were concentrated 24-fold with 3 kDa Amicon Ultra filter units (Sigma-Aldrich) to 0.5 mg/mL total protein concentrations prior to the analysis. Optical densities (absorbance at 450 nm) were measured in a plate reader (PerkinElmer, USA).

PCR assay

For the reverse transcription polymerase chain reaction (RT-PCR) assay, cells or tissues were collected in RNAlater (Thermo Fisher Scientific, USA) for the preservation of RNA molecules during storage. Total RNA from the collected cell or tissue samples was isolated with RNeasy Mini Kit (Qiagen, USA) according to the manufacturer's protocols. cDNA synthesis was carried out with RevertAid First Strand cDNA Synthesis Kit (Thermo Fisher Scientific) according to the manufacturer's protocol. The real-time PCR mixtures were set up with qPCRmix-HS SYBR (Evrogen, Russia); the reactions were carried out in a Bio-Rad iQ thermal cycler as primary denaturation 95 °C for 5 min followed by 40 cycles of denaturation 95 °C for 20 seconds, annealing 55–63 °C for 20 seconds and elongation 72 °C for 20 seconds. Raw data for the genes of interest were normalized against constitutively expressed reference genes *GAPDH* (*Gapdh*, glyceraldehyde-3-phosphate dehydrogenase) and *ACTB* (*Actb*, beta-actin). Expression levels were calculated by $2^{-\Delta\Delta C(T)}$ approach. The oligonucleotide sequences are given in Supplementary Table 1.

In vitro and *in vivo* study design

In vitro experiments involved SHSY-5Y neuroblastoma cell line. CM were applied at 4 h after hypoxia modeling to the final total protein concentration of 5 μg/mL. At 24 h after hypoxia modeling, cell survival was assessed by MTT and LDH tests, vital staining with propidium iodide and Hoechst 33342, and the levels of apoptosis-related gene expression. In the longer incubation experiments, CM were added every other day to the same final protein concentration. Formation of axons and dendrites was assessed by expression markers of neuritogenesis *MAP2* and *GAP43* and alterations in cell morphology on days 1, 3 and 7 of the experiment.

In vivo experiments involved adult male Wistar rats of 250–300 g body weight (n=34) purchased from AlCondi Ltd., Russia. All manipulations with the animals were approved by the Ethical Committee at N.I.

Pirogov Russian National Research Medical University. All *in vivo* experiments were carried out in accordance with EU Directive 2010/63/EU.

The experimental ischemic stroke was modeled by temporary occlusion of the right middle cerebral artery. At 24 h after the stroke, the animals (n=34) were randomized into 3 groups: control group (n=10) and CM recipients (n=12 each) to receive intra-arterial infusions of, respectively, the non-conditioned DMEM/F12-based medium, concentrated GPC-CM or NPC-CM to 50 μg/mL of total protein. Therapeutic effects were assessed the following parameters: survival, neurological deficit and the stroke volume immediately before the infusion (day 1) and on days 7, 14 and 30 post infusion (p/i). The animals were sacrificed at the end of the experiment (day 30 p/i). At the autopsy, the ischemized portions of the brain tissue were dissected into 3 fragments. One fragment was fixed in 10% formalin for paraffin sections, one was preserved in liquid nitrogen for cryosections, and one was preserved in RNAlater reagent for PCR analysis. Corresponding area from the unaffected contralateral hemisphere was dissected in the same way to be used as a control.

In vitro study of neuroprotective properties

Modeling of chemically induced hypoxia

SHSY-5Y cells were cultured in DMEM/F12 (PanEco) supplemented with 10% FBS (PanEco). One week prior to the addition of the mimetic, the cells were seeded in 12-well plates (Corning, USA) coated with collagen type I solution (Gibco) at 90×10^3 cells per well and incubated in Gibco Opti-MEM supplemented with 10 mM retinoic acid (Gibco) and 0.5% FBS (PanEco) for 2 days. The growth medium was subsequently replaced with DMEM/F12 (PanEco) supplemented with B-27 (to 1X, Gibco) and 50 ng/mL BDNF (PeproTech). At 72 prior to hypoxia, the medium was depleted of BDNF. The cells were exposed to 250 μM $CoCl_2$ for 4 h, washed with HBSS (PanEco) and replated in DMEM/F12 (PanEco) supplemented with B-27 (Gibco) [16].

Evaluation of cell survival

MTT ((3-(4,5-dimethylthiazol-2-yl)-2,5-diphenyltetrazolium bromide, PanEco) was added to the culture medium to a final concentration of 0.5 mg/mL. The measurements were carried out after 2 h incubation with MTT and subsequent dissolution of formazan crystals with DMSO (PanEco). Evaluation of necrosis rates by LDH tests was carried out by using LDH Activity Assay Kit (Sigma-Aldrich) according to the manufacturer's protocol. Optical densities (absorbance at 570/620 nm for MTT test or 450 nm for LDH test) were measured in a plate reader (PerkinElmer). Cell death rates were assessed by staining the cells with vital fluorescent dyes Hoechst 33342 (Sigma-Aldrich, 5 μg/mL for 30 min) and propidium iodide (Sigma-Aldrich, 1 μg/mL for 10 min) to visualize nuclear fragmentation and membrane integrity. The fluorescence patterns were observed and recorded with Axio Observer.D1 inverted fluorescence microscope equipped with AxioCam HRc (Carl Zeiss).

Assessment of neurite outgrowth

Formation of axons and dendrites was assessed by morphological examination combined with immunocytochemistry for βIII tubulin, and also by real-time PCR assay for the transcriptomic markers of neuritogenesis (*MAP2*, *GAP43*).

In vivo study of neuroprotective properties

Modeling of ischemic stroke

Transient occlusion of the middle cerebral artery in rats was performed by standard method (the procedure originally developed by Koizumi [17] and modified by Longa [18]). The animals were anesthesized with 2.5–3% isoflurane/97–97.5% air mixture. The right middle cerebral artery was temporary occluded with a silicone rubber-coated monofilament (diameter 0.19 mm, length 30 mm, diameter with coating 0.37±0.02 mm, coating length 3–4 mm; Doccol, USA) for 90 min. During the operation and until the emergence from anesthesia the body temperature was maintained at 37 °C with a warming pad.

Comparative assessment of the neurological deficit and functional recovery

Therapeutic effects of CM administration were determined by survival rates, infarct volume and neurological deficits as assessed by using the modified neurological severity scores (mNSS) for rodents [19] immediately before the infusion (day 1) and on days 7, 14 and 30 p/i.

Magnetic resonance imaging (MRI)

The imaging was accomplished in a 7T ClinScan small animal MRI system (Bruker BioSpin, USA). Intraoperative MRI (monitoring of the monofilament position, intracranial blood flow and hemorrhagic complications) was carried out as described previously [20]. For MRI evaluation of *in vivo* dynamics of the stroke volume, axial plane T2-weighted brain images (T2-WI) were acquired immediately before the infusion (day 0) and on days 7, 14 and 30 p/i. Quantitative reconstruction of the infarct volume on the basis of T2-WI was accomplished in ImageJ software (Wayne Rasband, National Institute of Mental Health, Bethesda, MD, USA) by calculating $V= (S_1+...+S_n) \times (h+d)$, where S values correspond to the infarct area measured in individual sections, h is slice thickness, and d is spacing between the slices.

Histology

The formalin-fixed tissues were dehydrated and embedded in paraffin and cut on a microtome. The 5–7 μm thick sections were positioned on gelatin-coated slides and dried at 37 °C for 24 h. The sections were deparafinized in xylene and rehydrated in 100°–70° ethanol series, stained with H&E, dehydrated and mounted. Pathohistological examination of the sections by light microscopy was carried out using Axio Observer.D1 equipped with AxioCam HRc (Carl Zeiss). Formation of new blood vessels at the site of injury was assessed in the images of the H&E stained histological sections at x400 magnification by using ImageJ software. Blood vessels were identified as hollow structures of characteristic morphology and red blood cells in the limina. The total number of blood vessels per sq mm of the section and the volume

density of blood vessels (estimated as the total cross-sectional area of blood vessels per sq mm of the section) were evaluated.

Immunohistochemistry

The tissues cryopreserved in liquid nitrogen were cryosectioned at a 4–5 μm thickness. The sections were pre-blocked in PBS with 0.3% Triton X-100 and 2% BSA for 1 h, incubated with anti-CD68 primary antibodies (ab125212, Abcam) at +4 °C overnight, washed and incubated with secondary antibodies (Alexa Fluor 488 conjugated, Invitrogen) for 60 min in the dark. The nuclei were counterstained with DAPI solution (1 μg/mL in PBS). The images were recorded with Axio Observer.D1 inverted fluorescence microscope equipped with AxioCam HRc (Carl Zeiss). Total counts of $CD68^+$ cells per sq mm of the section were determined with ImageJ software by counting the positively stained cells at x200 magnification.

Statistical analysis

The data were processed in SigmaPlot 12.5 software. Each single group included 3–5 independent experiments. Pairwise comparisons were carried out by t-test in the case of normal distribution or Mann Whitney test in the case of non-normal distribution. For multiple comparisons, one-way ANOVA with Holm-Sidak method was used for the cases of normal distribution, whereas ANOVA on ranks with Dunn's test was used for the cases of non-normal distribution. Differences at $p \leq 0.05$ were considered significant.

Results

Characterization of hiPSCs, NSCs, GPCs and NPCs

The obtained hiPSCs were morphologically similar to human embryonic stem cells with high nuclear-cytoplasmic ratio (Fig. 1A). The cells expressed pluripotency markers *OCT4, NANOG* and *SOX2*, and were immunopositive for OCT4 and NANOG transcription factors and SSEA4 and TRA-1-81 proteoglycans. The cells also showed the capacity of spontaneous differentiation into derivatives of any of the three germ layers (ectoderm, endoderm and mesoderm), which confirmed their pluripotency at the functional level (Fig. 1A, B). Culturing with appropriate inducers (see Section 2.1) afforded neural stem cells (NSCs) — small, densely growing cells prone to the formation of 3D rosette-like structures. The NSC phenotype was confirmed immunocytochemically and by PCR assay. NSCs expressed molecular markers of neural differentiation (*PAX6*, *SOX2* and *NES*) and were immunopositive for the corresponding proteins. Differentiation efficiency (as the proportion of PAX6-positive cells evaluated by flow cytometry) constituted 98±1.8% (Fig. 1C). Upon stimulation with glial inducers the cells acquired spindle-shaped morphology with uneven outlines and large oval nuclei. Stimulation of NSCs with neuronal inducers promoted the outgrowth of neurites up to three cell diameters long. Glial progenitor cells (GPCs) expressed *S100B* and *GFAP*, and 97±2.8% of them were S100B-positive. Neuronal progenitor cells (NPCs)

had smaller nuclei, expressed neuronal markers *TUBB3*, *MAP2* and *ENO2*, and 96±3.4% of them were βIII tubulin positive (Fig. 1D).

Comparative study of GPC and NPC secretomes

The NPC-conditioned media (NPC-CM) contained more protein species than GPC-conditioned media (GPC-CM). Of 304 protein species identified in NPC-CM, 136 (45%) were specific (i.e. not found in GPC-CM, Fig. 2A). A considerable number of NPC-CM-specific peptides reportedly exert neuroprotective properties (e.g. tissue inhibitor of metalloproteinases 2 (TIMP2), Wnt family member 5A, neuropilin-1, secretogranin-2, platelet-derived growth factor D [21–23]) and neurotrophic properties (e.g. ataxin 10, ephrin B1, fibroblast growth factor 8, glypicans 2, 4 and 6, netrin 1, neuroserpin 1, semaphorin 3C, neuronal pentraxin 2, basigin [24–28]). NPC secretomes also comprised apolipoproteins (which attenuate the activity of neutrophils [29,30]) and osteopontin (chemotactic protein involved in the activation of immune cells and cytokine production [31,32], Table 1).

Of 243 protein species identified in GPC-CM, 75 (31%) were specific (i.e. not found in NPC-CM, Fig. 2A), including important regulators of cell survival (growth arrest-specific protein 6, heat shock 70 kDa protein 4, heat shock 105 kDa protein, leukemia inhibitory factor, gremlin 1, Hsp70 interacting protein [21,33–35]) and axonal/dendritic growth (dynactin, thrombospondin 2, twinfilin 2, sorting nexin 3, prosaposin [36–40]). GPC secretomes also comprised growth and differentiation factor 15 and SH3 domain-binding glutamic acid-rich-like protein 3 known to exert pronounced anti-inflammatory effects [41,42] (Table 1).

Comparative analysis of GPC and NPC secretomes also revealed differences in representation for certain functional classes of proteins, e.g. the levels of transfer/carrier proteins (PC00219) and membrane traffic proteins (PC00150) in GPC secretomes were increased, respectively, 2.8-fold and 5-fold compared with NPCs (Fig. 2B).

Table 1. Secreted proteins of the hiPSC-derived neuronal and glial progenitor cells identified by proteomic approach.

Neuronal progenitor cells (NPCs)	Glial progenitor cells (GPCs)
Proteins involved in the regulation of apoptosis and cell survival	
apolipoprotein E (APOE)	
clusterin (CLU)	
cofilin 1 (CFL1)	
galectins 1 and 3 (LGALS1, LGALS3)	
midkine (MDK)	
14-3-3 proteins β/ (YWHAB), (YWHAE), γ (YWHAG), (YWHAH), (YWHAQ), ζ/ δ (YWHAZ)	
insulin-like growth factor-binding protein 3 (IGFBP3)	
thrombospondin 1 (THBS1)	
high-mobility group protein B1 (amphoterin, HMGB1)	
heat shock protein beta 1 (heat shock protein 27, HSPB1)	
heat shock 70 kDa protein 8 (HSPA8)	
phosphatidylethanolamine binding protein 1 (PEBP1)	
cathepsin D (CTSD)	
cysteine-rich angiogenic inducer 61 (CYR61)	
platelet-derived growth factor C (PDGFC)	
tumor protein, translationally-controlled 1 (TPT1)	
tissue inhibitor of metalloproteinases 1 (TIMP1)	
pigment epithelium-derived factor (SERPINF1)	
tissue inhibitor of metalloproteinases 2 (TIMP2)	heat shock 70 kDa protein 4 (HSPA4)
secretogranin-2 (chromogranin C, SCG2)	heat shock protein 105 kDa (HSPH1)
Wnt family member 5a (WNT5A)	Hsc70-interacting protein (ST13)
neuropilin-1 (NRP1)	leukemia inhibitory factor (LIF)
Ras homolog family member A (RHOA)	growth arrest-specific protein 6 (GAS6)
platelet-derived growth factor D (PDGFD)	gremlin 1 (GREM1)
	tetranectin (TETN)

Proteins involved in the regulation of axonal and dendrite outgrowth	
stathmin (STMN1)	
neuropilin 2 (NRP2)	
periostin (POSTN)	
vinculin (VCL)	
heat shock 90 kDa proteins and β (HSP90AA1, HSP90B1)	
agrin (AGRN)	
connective tissue growth factor (CTGF)	
fibulin 1 (FBLN1)	
protease nexin 1 (SERPINE2)	
profilin 1 (PFN1)	
secreted protein acidic and rich in cysteine (SPARC)	
growth factor receptor-bound protein 2 (GRB2)	
ataxin-10 (ATXN10)	dynactin (DCTN)
ephrin-B1 (EFN1B)	thrombospondin 2 (THBS2)
ezrin (EZR)	disintegrin and metalloproteinase domain-containing protein 19 (ADAM19)
fibroblast growth factor 8 (FGF8)	phosphatidylinositol transfer proteins alpha and beta (PITPNA, PITPNB)
glycopicans 2, 4 and 6 (GPC2, GPC4, GPC6)	twinfilin 2 (TWF2)
netrin 1 (NTN1)	sorting nexin 3 (SNX3)
neuroserpin 1 (SERPINI1)	prosaposin (PSAP)
semaphorin 3C (SEMA3C)	
neuronal pentraxin 2 (NPTX2)	
basigin (BSG)	
C1q-related factor (CRF)	
Proteins with immunomodulatory properties	
cathepsin B (CTSB)	
macrophage-capping protein (CAPG)	
macrophage migration inhibitory factor (MIF)	
CYFIP-related Rac1 interactor B (FAM49B, CYRIB)	

syndecan binding protein (SDCBP)	
Rab GDP dissociation inhibitor beta (GDI2)	
pentraxin-related protein (PTX3)	
coactosin-like protein 1 (COTL1)	
cystatins B and C (CSTB, CST□)	
serpin B6 (SERPINB6)	
annexin A1 (ANXA1)	collectin subfamily member 12 (COLEC12)
nectin 2 (NECTIN2)	vitamin D binding protein (VTDB)
meteorin-like protein (METRNL)	importin subunit beta 1 (KPNB1)
moesin (MSN)	Toll-interacting protein (TOLLIP)
apolipoprotein A1 (APOA1)	S100-A11 protein (S100A11)
28 kDa heat- and acid-stable phosphoprotein (PDAP1)	growth and differentiation factor 15 (GDF15)
osteopontin (SPP1)	SH3 domain-binding glutamic acid-rich-like protein 3 (SH3BGRL3)
Ras-related protein Rap-1b (RAP1B)	
Proteins involved in tissue repair	
GM2 ganglioside activator protein (GM2A)	
gelsolin (GSN)	
glia maturation factor beta (GMFB)	
pleiotrophin (PTN)	
Proteins involved in redox reactions	
thioredoxin (TXN)	
thioredoxin domain-containing protein 17 (TXD17)	
sulfhydryl oxidase 1 (QSOX1)	
peroxiredoxins 1, 2, 5 and 6 (PRDX1, PRDX2, PRDX5, PRDX6)	
peroxidasin homolog (PXDN)	
peptidyl-glycine alpha-amidating monooxygenase (PAM)	
glyoxylate and hydroxypyruvate reductase (GRHPR)	lysyl oxidase homolog 1 (LOXL1)
catalase (CAT)	peroxiredoxin 4 (PRDX4)

	superoxide dismutase 1 (SOD1)
	protein disulfide-isomerase (P4HB)
	thioredoxin domain-containing protein 5 (TXNDC5)
	glutathione S-transferase omega 1 (GSTO1)

Neurotrophins are secretory proteins which maintain the viability of neurons and stimulate their development and activity. Neurotrophins were not identified by proteomic approach apparently due to their low concentrations in CM; however, their concentrations were within the sensitivity limit of ELISA. Neurotrophin concentrations in the undiluted GPC-CM and NPC-CM were of the pg/mL order, which is lower than required for therapeutic activity. At the same time, concentrations of BDNF, NGF, CNTF and GDNF in GPC-CM were, respectively, 19-, 12-, 18- and 3-fold higher than in NPC-CM (Fig. 2C).

Selective differential profiling of gene expression in progenitor cell cultures was performed on the basis of the identified cell type-specific secreted proteins in combination with the literary data on their functions. A number of genes differentially expressed by NPCs and GPCs were identified, including *YWHAB* (14-3-3 protein beta/alpha), *CLU* (clusterin), *HSPB1* (heat shock protein beta 1), *HSPA8* (heat shock 70 kDa protein 8), *SERPINF1* (pigment epithelium-derived factor), *HSP90AA1* (heat shock 90kDa protein 1, alpha), *MIF* (macrophage migration inhibitory factor), *HDGF* (hepatoma-derived growth factor) and *PTN* (pleiotrophin). Transcription levels of *HDGF*, *HSPA8* and *PTN* were higher in NPCs compared with GPCs, whereas transcription levels of *SERPINF1* and *HSPB1* were higher in GPCs. It should be noted that *BDNF* (brain-derived neurotrophic factor), *CNTF* (ciliary neurotrophic factor), *NGF* (nerve growth factor), *GDNF* (glial cell-derived neurotrophic factor), *APOE* (apolipoprotein E) and *MDK* (midkine) were expressed by both NPCs and GPCs, but at lower levels compared with other studied genes. At the same time, expression levels of *BDNF*, *CNTF*, *NGF, GDNF* and *MDK* in GPCs were higher compared with NPCs (Fig. 2C). GPCs showed high expression levels of *GREM1* (gremlin 1), *GAS6* (growth arrest-specific protein 6), *LIF* (leukemia inhibitory factor), *TWF2* (twinfilin 2), *SNX3* (sorting nexin 3), *MYDGF* (myeloid-derived growth factor), *TGFB2* (transforming growth factor beta 2) and *GDF15* (growth and differentiation factor 15) (Fig. 2D). In NPCs, expression of these genes was low or undetectably low. At the same time, a number of genes including *FGF8* (fibroblast growth factor 8), *NTN1* (netrin 1), *NPTX2* (neuronal pentraxin 2), *EFBN1* (ephrin B1), *SERPINI1* (neuroserpin 1) and *VGF* (neuro-endocrine specific protein VGF) were expressed specifically by NPC cultures (Fig. 2D).

Evaluation of neuroprotective effects of NPC-CM and GPC-CM in the in vitro model

Modeling of hypoxia in SH-SY5Y cells by the 4 h exposure to 250 μM $CoCl_2$ dramatically affected their survival as indicated by MTT tests carried out at 24 h after the treatment. In the absence of NPC-CM or GPC-CM, hypoxia caused a reduction in the numbers of viable cells by 73±4.1% and an increase in the amounts of LDH released from necrotic cells by 11.7±2.4% as compared with the no-hypoxia controls. The exposure to NPC-CM increased the survival of SH-SY5Y cells by 9.26±2.8%; however, the amounts of cell-free LDH measured after the exposure to NPC-CM and after hypoxia were similar. By contrast, the

exposure to GPC-CM not only increased the SH-SY5Y cell survival by 25.4±6.1% but also promoted a reduction in the levels of cell-free LDH in the culture medium by 8.7±2.7% compared with the $CoCl_2$ treated cultures (Fig. 3A).

In the aftermath of $CoCl_2$ – induced hypoxia, the cells died predominantly by apoptosis (55.4±3.9 %) and to a lesser extent by necrosis (16.6±2.5%, Fig. 3A). Treatment of the cells with GPC-CM reduced the apoptotic cell numbers to 35.1±2.8% and necrotic cell numbers to 10.2±3.9%. Treatment of the cells with NPC-CM reduced the apoptotic cell numbers to 42.2±3.0% only and caused no significant reduction in the necrotic cell numbers.

Cell viability was additionally assessed by expression of apoptosis-related genes — pro-apoptotic *BAX* and anti-apoptotic *BCL2*, which encode regulatory proteins of the same family. At 24 h after the $CoCl_2$ – induced hypoxia, the level of *BCL2* expression was reduced 6.2-fold whereas the level of *BAX* expression was increased 2.3-fold as compared with the no-hypoxia control. The treatment with GPC-CM promoted a 2-fold reduction in *BAX* expression and a 3.7-fold increase in *BCL2* expression as compared with the $CoCl_2$ treated cultures. Interestingly, in terms of *BAX*/*BCL2* expression, the effect of treatment with NPC-CM was similar: it promoted a 2-fold reduction in *BAX* expression and a 3.2-fold increase in *BCL2* expression as compared with the $CoCl_2$ treated cultures (Fig. 3A).

In the no-hypoxia controls, the cells retained typical SH-SY5Y morphology with long βIII tubulin-immunopositive outgrowths. The $CoCl_2$-induced hypoxia caused degeneration of axons and dendrites: neuronal bodies were prominent, but the neurites were missing or shortened (Fig. 3B).

In the aftermath of $CoCl_2$-induced hypoxia without CM treatment, expression levels of *MAP2* and *GAP43* were significantly reduced during the entire period of observation (days 1, 3 and 7) as compared with the no-hypoxia control (Fig. 4C). On days 1 and 3, the NPC-CM treated cell cultures showed no signs of neurite outgrowth. By day 7, however, the NPC-CM treated cells developed short processes while having significantly elevated *MAP2* and *GAP43* expression levels as compared with the $CoCl_2$ treated cultures. Neurotrophic effects of GPC-CM were more pronounced: regeneration of axons and dendrites in the GPC-CM treated cultures was evident during the entire period of observation (days 1, 3 and 7). On day 7, *MAP2* and *GAP43* expression levels in the GPC-CM treated cells were significantly elevated as compared with both the NPC-CM and $CoCl_2$ treated cultures (Fig. 4C).

Therapeutic effects of the intra-arterial infusion of NPC-CM and GPC-CM in the experimental ischemic stroke

Kaplan-Meier survival curves for three groups (NPC-CM treated, GPC-CM treated and the non-conditioned media-treated control) are shown in Fig. 4A. All deaths occurred within 3 days after the stroke and were associated with vasogenic cerebral edema. CM infusions had no effect on survival.

Neurological severity scores (mNSS) were recorded at the following time points: immediately before the infusion (day 1), and on days 7, 14 and 30 p/i. Neurological deficit reached its maximum by 24 h after the acute focal ischemia modeling in all groups; its progression was associated with the cerebral infarct development. After that, the neurological deficit underwent regression in all groups; the highest rates of functional recovery were observed during the initial 2 weeks of the experiment. The scores for the GPC-CM group on days 14 and 30 p/i were, respectively, 1.5-times and 1.6-times lower as compared with the control group; these differences were significant (Fig. 4 B). By contrast, no significant differences in mNSS between the NPC-CM group and the control group were observed during the experiment. The data indicate enhanced functional recovery of brain function in response to the infusion of GPC-CM during the acute period of ischemic stroke.

The stroke volume was evaluated by MRI, with T2-weighted brain magnetic resonance images acquired at different time points used for the evaluation. Reduction in the infarct volume was pronounced in all groups; no significant differences between the groups were revealed in the course of observation (Fig. 4C, D).

To understand the CM-mediated therapeutic effects at molecular level, expression of apoptosis- and inflammation-related molecular markers in brain tissues was studied by PCR-based assay (Fig. 5). The GPC-CM group showed significantly reduced expression of the pro-apoptotic gene *Bax* compared with the control group. By contrast, expression levels of *Bax* in the ischemized tissue of the NPC-CM group were 2.4-times higher as compared with the intact brain tissue in contralateral cerebral hemisphere (IH) and the GPC-CM group; these differences were also significant. At the same time, no significant differences in *Bcl2* expression were observed between the groups (Fig. 5A).

Vascular necrosis causes secondary damage to brain parenchyma due to the continuous inflammatory reaction accompanied by the elevated expression of *Tnf* gene. Infusion of GPC-CM specifically reduced *Tnf* expression in the affected brain parenchyma; the difference with the control was statistically significant. In addition, expression levels of the anti-inflammatory cytokine genes *Il4*, *Il10* and *Il13* were significantly elevated in the ischemized brain tissues of GPC-CM treated animals compared with the control group. By contrast, expression levels of *Tnf*, *Il4*, *Il10* and *Il13* in the ischemized brain tissues of NPC-CM treated animals were comparable with the control group (Fig. 5A). Expression levels of *Il1b* and *Il6* in all groups were similar.

As demonstrated by histological study, the infusion of GPC-CM supported neoangiogenesis. The counts of newly formed perfused blood vessels in the ischemized brain tissues of GPC-CM treated animals were the highest; the difference with the control group was significant ($p < 0.05$, Fig. 5B, C).

CD68 is a cell surface glycoprotein highly expressed on phagocytic cells of the resident microglia and infiltrating monocytic macrophages. Accumulation of CD68 positive cells in the ischemized brain area was detected at the autopsy on day 30 p/i in all groups. However, this effect was significantly alleviated in GPC-CM treated animals, as the numbers of accumulated phagocytic cells were lower compared with

other groups. No such alleviation was observed in the NPC-CM group where the counts of CD68+ cells in the damaged area were significantly higher (Fig. 5B, C).

Discussion

hiPSC-derived NPCs and GPCs produce and secrete numerous regulatory proteins and peptides. NPC and GPC secretomes partially overlap, but large proportions of proteins in their secretomes are highly specific. Although no straightforwardly matching data are available from the literature, the obtained results can be indirectly compared with other studies. For instance, the obtained NPC secretory profiles show 71% overlap with the results of Mendes-Pinheiro *et al.* (2018), who applied proteomic approach to the primary cultures of human neuronal progenitors and identified 538 secreted proteins [43]. Significant overlaps of the obtained GPC secretory profiles with the corresponding data for primary cultures of human astrocytes should be noted as well [44–49].

Both NPC and GPC cultures secreted low amounts of neurotrophins (BDNF, CNTF, NGF). However, at the mRNA level, GPC cultures showed higher expression of *BDNF*, *CNTF* and *NGF*, which is consistent with higher rates of neurotrophin secretion by GPC cultures reported elsewhere [50–52].

GPC-CM promoted cell survival and facilitated neurite outgrowth in SHSY-5Y cells after 4 h of acute hypoxia (modeled by exposure to $CoCl_2$) more efficiently than NPC-CM.

Intra-arterial infusion of GPC-CM during the recovery after experimental ischemic stroke in rat model was advantageous. Compared with NPC-CM and the non-conditioned media, GPC-CM accelerated functional recovery of the brain: it reduced the neurological deficit and downregulated the expression of pro-apoptotic gene *Bax*. Although the GPC-CM administration had no significant effects on the infarct volume dynamics, its anti-inflammatory and pro-angiogenic effects were pronounced. These effects included decreased counts of phagocytic cells (microglia/macrophages), elevated expression levels of pro-inflammatory cytokine genes (*Il4, Il10*, *Il13*), reduced expression level of *Tnf* and increased numbers of newly formed blood vessels. The NPC-CM infusions had no pronounced functional effects. Moreover, expression levels of *Bax* and the counts of $CD68^+$ cells within the affected brain area of the NPC-CM treated animals were significantly higher than for the GPC-CM treated animals.

Thus, the results indicate pronounced neuroprotective, anti-inflammatory and pro-angiogenic properties of GPC secretomes as compared with NPC secretomes. The difference is apparently related to unique secretory profiles of the glial progenitor cells. One of the major causes of cell death in hypoxia is the accumulation of reactive oxygen species which results in oxidative stress [53,54]. According to the presented proteomic data, GPC secretomes show stronger involvement in the redox chemical processes than NPC secretomes. The difference in cytoprotective properties between the two cultures can be also due to higher representation of anti-apoptotic signal molecules in GPC-CM (e.g. LIF, HSPA4, HSPH1, GREM1 and GAS6). The pronounced neurotrophic effects of GPC-CM can be mediated by proteins specifically involved in the growth of axons and dendrites (e.g. TWF2, PSAP, SNX3, THBS2); they can be

also related to higher secretion levels of neurotrphins (BDNF, NGF, GDNF, CNTF). Anti-inflammatory action of GPC-CM in the experimental model of ischemic stroke can be explained by the presence of COLEC12, KPNB1, TOLLIP, GDF15 and SH3BGRL3 proteins, whereas its pro-angiogenic effects in the same model can be associated with the presence of MYDGF, HDGF and TGF β2.

The obtained results on neuroprotective, anti-inflammatory and pro-angiogenic properties of GPC-CM are consistent with previous reports demonstrating the efficiency of stem and progenitor cell-conditioned media *in vitro* и *in vivo*. Lu *et al.* (2011) demonstrated neuroprotective effects of adipose tissue-derived mesenchymal stem cell-conditioned media (MSC-CM) on PC12 cells under conditions of glutamate excitotoxicity [55]. The capacity MSC-CM to induce neurite outgrowth in SH-SY5Y cells was demonstrated by Pires *et al.* (2014) [56]. Wilkins *et al.* (2009) demonstrated that the incubation of cortical neurons with the bone marrow MSC-CM significantly increased survival via inhibition of apoptosis [57]. The therapeutic effects of CM were also evaluated *in vivo*. For instance, administration of NSC-conditioned media to the rats with experimental ischemic stroke promoted alleviation of neurological deficit and reduction in the infarct volume compared with the control group [58]. Intra-venous infusion of the bone marrow MSC-CM to the rats with experimental ischemic stroke significantly enhanced functional recovery and alleviated the microglial/macrophage infiltration of brain tissue [59]. As demonstrated by Hicks *et al.* (2013), the transplanted primary NSCs actively produce angiopoietin 1 (Ang1) which promotes an increase in the amount of microvessels in the ischemized area of the brain [60]. However, the effects of secretomes of the iPSC-derived neuronal and glial progenitors on the viability and structural organization of the SH-SY5Y cell cultures, as well as the recovery of the brain tissue after experimental ischemic stroke are reported here for the first time.

This study also firstly demonstrates the effects of the hiPSC-derived GPC-CM and NPC-CM on the preservation and outgrowth of axons and dendrites in SHSY-5Y cells under model hypoxic conditions (conferred by $CoCl_2$ exposure). The results indicate neuroprotective effects of GPC-CM on SHSY-5Y cells as assessed by a number of parameters including neurite outgrowth. Consistently with the *in vitro* experiments, GPC secretomes significantly enhance functional recovery of the brain after the experimental ischemic stroke, apparently due to the specific content of secreted proteins. The hiPSC-derived glial progenitors represent a promising candidate for clinical studies as they can be obtained in virtually unlimited numbers from the patient own cells (e.g. dermal fibroblasts) and used as autologous transplants. The obtained results indicate the importance of further investigation of the properties of the human iPSC-derived neuronal and glial progenitor cells for the therapies of neurodegenerative and cerebrovascular disorders.

Conclusion

Conventional therapies for vascular diseases of the brain do not allow complete functional recovery of damaged tissues, hence the modest success of neurological rehabilitation. Post-ischemic repair of brain tissue remains a primary challenge for modern medicine.

Secretory activity of the hiPSC-derived NPCs and GPCs was studied by enzyme-linked immunosorbent and proteomic approaches. The study reveals significant differences in representation of regulatory proteins (neurotrophins, growth factors, cytokines, heat shock proteins) in GPC and NPC secretomes. The findings provide information on paracrine mechanisms of neuroprotection, angiogenesis and anti-inflammatory activity. The data indicate more pronounced paracrine effects of GPCs compared with NPCs, presumably due to the activity of specific proteins found in GPC-CM and absent from NPC-CM, e.g. LIF, HSPA4, HSPH1, TWF2, PSAP, SNX3, THBS2, as well as MYDGF, HDGF and TGF β2. This study nominates the hiPSC-derived glial progenitor cultures as a promising affordable source of proteins and peptides for the therapy of vascular and neurodegenerative diseases of the central nervous system; importantly, such cultures can be obtained directly from the patient (using the induced pluripotent stem cell-based protocols). The results on neuroprotective, anti-inflammatory and angiogenic properties of the hiPSC-derived glial progenitor cultures may facilitate development of nootropic formulations on their basis.

Abbreviations

hiPSCs: Human induced pluripotent stem cells

NSCs: Neural stem cells

NPCs: Neuronal progenitor cells

GPCs: Glial progenitor cells

MSC: Mesenchymal stem cell

CM: Conditioned media

GPC-CM: Glial progenitor cell - conditioned media

NPC-CM: Neuronal progenitor cell - conditioned media

MSC-CM: Mesenchymal stem cell - conditioned media

GDNF: Glial cell-derived neurotrophic factor

BDNF: Brain-derivedneurotrophic factor

NGF: Nerve growth factor

CNTF: Ciliary neurotrophic factor

FGF-2: Fibroblast growth factor-2.

EGF: Epidermal growth factor

LDH: Lactate dehydrogenase

DAPI: 4', 6-diamidino-2-phenylindole

Declarations

Ethics approval and consent to participate

Skin biopsies from donors were taken at the Research Centre for Medical Genetic after patients signed informed consent. The research was approved by the local Ethical Committee. All *in vivo* experiments were carried out in accordance with EU Directive 2010/63/EU and were approved by the Ethical Committee at N.I. Pirogov Russian National Research Medical University.

Consent for publication

Not applicable

Competing interests

The authors declare that they have no competing interests.

Funding

The study was supported by the Ministry of Science and Higher Education within the State assignment for the Research Centre for Medical Genetics.

Authors' contributions

Not applicable

Acknowledgements

We acknowledge Ekaterina Kirienko for excellent technical assistance. Mass spectra were recorded on the equipment of "Human Proteome" core facility (Institute of Biomedical Chemistry, Moscow, Russia).

References

1. Calvo-Anguiano G, Lugo-Trampe JJ, Camacho A, et al. Comparison of specific expression profile in two in vitro hypoxia models. Experimental and Therapeutic Medicine. 2018;15(6): 4777-84. https://www.spandidos-publications.com/etm/15/6/4777
2. Singh VK, Kalsan M, Kumar N, Saini A, Chandra R, et al. Induced pluripotent stem cells: Applications in regenerative medicine, disease modeling, and drug discovery. Frontiers in cell and developmental biology. 2015;3:2.

3. Gnecchi M, Danieli P, Malpasso G, Ciuffreda MC, et al. Paracrine mechanisms of mesenchymal stem cells in tissue repair. Methods Mol Biol. Humana Press Inc; 2016.123–46.
4. Baraniak PR, McDevitt TC. Stem cell paracrine actions and tissue regeneration. Regenerative medicine. 2010;5(1):121-43.
5. Kumar P, Kandoi S, Misra R, Verma RS, et al. The mesenchymal stem cell secretome: A new paradigm towards cell-free therapeutic mode in regenerative medicine. Cytokine Growth Factor Rev. Elsevier Ltd; 2019.1–9.
6. Khubutiya MS, Vagabov AV, Temnov AA, Sklifas AN, et al. Paracrine mechanisms of proliferative, anti-apoptotic and anti-inflammatory effects of mesenchymal stromal cells in models ofacute organ injury. Cytotherapy. Informa Healthcare; 2014.579–85.
7. Pawitan JA. Prospect of Stem Cell Conditioned Medium in Regenerative Medicine. BioMed research international. 2014;2014:1-14. http://dx.doi.org/10.1155/2014/965849
8. Faezi M, Nasseri Maleki S, Aboutaleb N, Nikougoftar M. The membrane mesenchymal stem cell derived conditioned medium exerts neuroprotection against focal cerebral ischemia by targeting apoptosis. Journal of chemical neuroanatomy. 2018;94:21–31.
9. Tsai MJ, Tsai SK, Hu BR, Liou DY, Huang SL, Huang MC, et al. Recovery of neurological function of ischemic stroke by application of conditioned medium of bone marrow mesenchymal stem cells derived from normal and cerebral ischemia rats. Journal of biomedical science. 2014;21(1):1-12. http://www.jbiomedsci.com/content/21/1/5
10. Chambers SM, Fasano CA, Papapetrou EP, Tomishima M, Sadelain M, Studer L. Highly efficient neural conversion of human ES and iPS cells by dual inhibition of SMAD signaling. Nat Biotechnol. 2009;27:275–80.
11. Shutova M V., Chestkov I V., Bogomazova AN, Lagarkova MA, Kiselev SL. Generation of iPS Cells from Human Umbilical Vein Endothelial Cells by Lentiviral Transduction and Their Differentiation to Neuronal Lineage. Humana Press; 2011. 133–49.
12. Liu H, Zhang SC. Specification of neuronal and glial subtypes from human pluripotent stem cells. Cellular and Molecular Life Sciences. 2011;68(24):3995-4008.
13. TCW J, Wang M, Pimenova AA, Bowles KR, Hartley BJ, Lacin E, et al. An Efficient Platform for Astrocyte Differentiation from Human Induced Pluripotent Stem Cells. Stem Cell Reports. 2017;9:600–14.
14. Vaudel M, Barsnes H, Berven FS, Sickmann A, Martens L. SearchGUI: An open-source graphical user interface for simultaneous OMSSA and X!Tandem searches. Proteomics. 2011.11(5):996-9. http://doi.wiley.com/10.1002/pmic.201000595
15. Huang D, Sherman B, Lempicki RA. Bioinformatics enrichment tools: paths toward the comprehensive functional analysis of large gene lists. Nucleic acids research. 2009;37(1):1-13. https://academic.oup.com/nar/article-abstract/37/1/1/1026684
16. Presgraves SP, Ahmed T, Borwege S, Joyce JN. Terminally differentiated SH-SY5Y cells provide a model system for studying neuroprotective effects of dopamine agonists. Neurotox Res.

2003;5:579–98.

17. Koizumi J. Experimental studies of ischemic brain edema. 1. A new experimental model of cerebral embolism in rats in which recirculation can be introduced in the ischemic area. Jpn J Stroke. 1986;8:1–8.
18. Longa EZ, Weinstein PR, Carlson S, Cummins R. Reversible middle cerebral artery occlusion without craniectomy in rats. Stroke. 1989;20:84–91.
19. Si D, Li J, Liu J, Wang X, Wei Z, Tian Q, et al. Progesterone protects blood-brain barrier function and improves neurological outcome following traumatic brain injury in rats. Exp Ther Med. Spandidos Publications; 2014;8:1010–4.
20. Gubskiy IL, Namestnikova DD, Cherkashova EA, Chekhonin VP, Baklaushev VP, Gubsky L V., et al. MRI Guiding of the Middle Cerebral Artery Occlusion in Rats Aimed to Improve Stroke Modeling. Transl Stroke Res. 2018;9:417–25.
21. Moon C, Liu BQ, Kim SY, Kim EJ, Park YJ, Yoo JY, et al. Leukemia inhibitory factor promotes olfactory sensory neuronal survival via phosphoinositide 3-kinase pathway activation and Bcl-2. J Neurosci Res. 2009;87:1098–106.
22. Shi Y, Zhu N, Liu C, Wu H, Gui Y, Liao D, et al. Wnt5a and its signaling pathway in angiogenesis. Clinica Chimica Acta. 2017;471:263-269. https://www.sciencedirect.com/science/article/pii/S0009898117302437
23. Waragai M, Nagamitsu S, Xu W, Yu JL, Lin X, Ashizawa T. Ataxin 10 induces neuritogenesis via interaction with G-protein β2 subunit. J Neurosci Res. 2006;83:1170–8.
24. Moreno-Flores MT, Martín-Aparicio E, Ávila J, Díaz-Nido J, Wandosell F. Ephrin-B1 promotes dendrite outgrowth on cerebellar granule neurons. Molecular and Cellular Neuroscience.2002;20(3):429-46. https://www.sciencedirect.com/science/article/pii/S1044743102911280
25. Tanaka M, Ohashi R, Nakamura R, Shinmura K, Kamo T, Sakai R, et al. Tiam1 mediates neurite outgrowth induced by ephrin-B1 and EphA2. EMBO J. 2004;23:1075–88.
26. Kurosawa N, Chen GY, Kadomatsu K, Ikematsu S, Sakuma S, Muramatsu T. Glypican-2 binds to midkine: The role of glypican-2 in neuronal cell adhesion and neurite outgrowth. Glycoconj J. 2001;18:499–507.
27. Farhy-Tselnicker I, van Casteren AC, Lee A, Chang VT, Aricescu AR, Allen NJ. Astrocyte-secreted glypican 4 regulates release of neuronal pentraxin 1 from axons to induce functional synapse formation. Neuron. 2017;96(2):428-445. https://www.sciencedirect.com/science/article/pii/S0896627317309224
28. Bottazzi B, Inforzato A, Messa M, Barbagallo M, Magrini E, Garlanda C, Mantovani A. The pentraxins PTX3 and SAP in innate immunity, regulation of inflammation and tissue remodelling. Journal of hepatology. 2106;64(6):1416-27. https://www.sciencedirect.com/science/article/pii/S016882781600163X
29. Blackburn WD, Dohlman JG, Venkatachalapathi Y V, Pillion DJ, Koopman WJ, et al Apolipoprotein AI decreases neutrophil degranulation and superoxide production. Journal of lipid

research.1991;32(12):1911-18.

30. Furlaneto CJ, Ribeiro FP, Hatanaka E, Souza GM, Cassatella MA, Campa A. Apolipoproteins A-I and A-II downregulate neutrophil functions. Lipids. American Oil Chemists Society. 2002;37:925–8.
31. Wang KX, Denhardt DT. Osteopontin: Role in immune regulation and stress responses. Cytokine & growth factor reviews. 2008;19(5-6):333-45.
32. Chen W, Ma Q, Suzuki H, Hartman R, Tang J, Zhang JH. Osteopontin reduced hypoxia-ischemia neonatal brain injury by suppression of apoptosis in a rat pup model. Stroke. 2011;42:764–9.
33. Gil Lorenzo AF, Bocanegra V, Benardon ME, Cacciamani V, Vallés PG. Hsp70 regulation on Nox4/p22phox and cytoskeletal integrity as an effect of losartan in vascular smooth muscle cells. Cell Stress Chaperones. 2014;19:115–34.
34. Phani S, Jablonski M, Pelta-Heller J, Cai J, et al. Brain research. 2013;1500:88-98. https://www.sciencedirect.com/science/article/pii/S0006899313000668
35. Mosser DD, Caron AW, Bourget L, Denis-Larose C, Massie B. Role of the human heat shock protein hsp70 in protection against stress-induced apoptosis. Molecular and cellular biology. 1997;17(9):5317-27.
36. Yamada S, Uchimura E, Ueda T, et al. Biochemical and biophysical research communications. 2007;363(4): 926-30. https://www.sciencedirect.com/science/article/pii/S0006291X07020323
37. Kotani Y, Matsuda S, Sakanaka M, Kondoh K, Ueno S, Sano A. Prosaposin Facilitates Sciatic Nerve Regeneration In Vivo. J Neurochem. 2002;66:2019–25.
38. Tsuboi K, Hiraiwa M, research JO-D brain, 1998 undefined. Prosaposin prevents programmed cell death of rat cerebellar granule neurons in culture. Developmental brain research. 1998;110(2):249-55. https://www.sciencedirect.com/science/article/pii/S0165380698001096
39. Mizutani R, Yamauchi J, Kusakawa S, et al. Sorting nexin 3, a protein upregulated by lithium, contains a novel phosphatidylinositol-binding sequence and mediates neurite outgrowth in N1E-115 cells. Cellular signalling. 2009;21(11):1586-94. https://www.sciencedirect.com/science/article/pii/S0898656809002022
40. Hoffman J, O'Shea KS. Thrombospondin expression in nerve regeneration I. Comparison of sciatic nerve crush, transection, and long-term denervation. Brain research bulletin. 1999;48(4):413-20. https://www.sciencedirect.com/science/article/pii/S0361923099000210
41. Xu C, Zheng P, Shen S, Xu Y, Wei L, Gao H, et al. FEBS letters. 2005;579(13):2788-94. https://www.sciencedirect.com/science/article/pii/S0014579305004709
42. Strelau J, Sullivan A, Bö Ttner M, Lingor P, Falkenstein E, Suter-Crazzolara C, et al. Growth/differentiation factor-15/macrophage inhibitory cytokine-1 is a novel trophic factor for midbrain dopaminergic neurons in vivo. Journal of Neuroscience. 2000;20(23):8597-603.
43. Mendes-Pinheiro B, Teixeira FG, Anjo SI, Manadas B, Behie LA, Salgado AJ. Secretome of Undifferentiated Neural Progenitor Cells Induces Histological and Motor Improvements in a Rat Model of Parkinson's Disease. Stem cells translational medicine. 2018;7(11):829-38. http://doi.wiley.com/10.1002/sctm.18-0009

44. Kim JH, Afridi R, Lee WH, Suk K. Proteomic examination of the neuroglial secretome: lessons for the clinic. Expert Review of Proteomics; 2020. 1-14.
45. Jha MK, Kim J-H, Suk K. Proteome of brain glia: The molecular basis of diverse glial phenotypes. Proteomics. 2014;14(4-5):378-98. http://doi.wiley.com/10.1002/pmic.201300236
46. Suk K. Combined analysis of the glia secretome and the CSF proteome: Neuroinflammation and novel biomarkers. Expert Rev. Proteomics; 2010. 263–74.
47. Delcourt N, Jouin P, Poncet J, Demey E, Mauger E, Bockaert J, et al. Difference in mass analysis using labeled lysines (DIMAL-K): A new, efficient proteomic quantification method applied to the analysis of astrocytic secretomes. Mol Cell Proteomics. 2005;4:1085–94.
48. Han D, Jin J, Woo J, Min H, Kim Y. Proteomic analysis of mouse astrocytes and their secretome by a combination of FASP and StageTip-based, high pH, reversed-phase fractionation. Proteomics. 2014;14(13-14):1604-9.http://doi.wiley.com/10.1002/pmic.201300495
49. Verkhratsky A, Matteoli M, Parpura V, Mothet J, Zorec R, et al. Astrocytes as secretory cells of the central nervous system: idiosyncrasies of vesicular secretion. The EMBO journal. 2016;35(3):239-57. https://onlinelibrary.wiley.com/doi/abs/10.15252/embj.201592705
50. Kuno R, Yoshida Y, Nitta A, Nabeshima T, Wang J, Sonobe Y, et al. The role of TNF-alpha and its receptors in the production of NGF and GDNF by astrocytes. Brain Res. Elsevier; 2006;1116:12–8.
51. Gozes I, Furman S, Steingart RA, Mandel S, Hauser JM, Brenneman DE. Subcellular localization and secretion of activity-dependent neuroprotective protein in astrocytes. Neuron Glia Biol. 2004;1:193–9.
52. Jha MK, Kim JH, Song GJ, Lee WH, Lee IK, Lee HW, et al. Functional dissection of astrocyte-secreted proteins: Implications in brain health and diseases. Progress in neurobiology. 2018;162:37-69.
53. Chamorro Á, Dirnagl U, Urra X, Planas AM. Neuroprotection in acute stroke: Targeting excitotoxicity, oxidative and nitrosative stress, and inflammation. The Lancet Neurology. 2016;15(8):869-81.
54. Yang C, Ling H, Zhang M, Yang Z, Wang X, Zeng F, et al. Oxidative stress mediates chemical hypoxia-induced injury and inflammation by activating NF-κb-COX-2 pathway in HaCaT cells. Mol Cells. 2011;31:531–8.
55. Lu S, Lu C, Han Q, Li J, Du Z, Liao L, et al. Adipose-derived mesenchymal stem cells protect PC12 cells from glutamate excitotoxicity-induced apoptosis by upregulation of XIAP through PI3-K/Akt activation. Toxicology. 2011;279(1-3):189-95. https://www.sciencedirect.com/science/article/pii/S0300483X10005354
56. Pires AO, Neves-Carvalho A, Sousa N, Salgado AJ. The Secretome of Bone Marrow and Wharton Jelly Derived Mesenchymal Stem Cells Induces Differentiation and Neurite Outgrowth in SH-SY5Y Cells. Stem cells international. 2014;2014:1-10. http://dx.doi.org/10.1155/2014/438352
57. Wilkins A, Kemp K, Ginty M, Hares K, et al. Human bone marrow-derived mesenchymal stem cells secrete brain-derived neurotrophic factor which promotes neuronal survival in vitro. Stem cell research. 2009;3(1):63-70. https://www.sciencedirect.com/science/article/pii/S1873506109000282
58. Yang HN, Wang C, Chen H, Li L, Ma S, Wang H, et al. Neural stem cell-conditioned medium ameliorated cerebral ischemia-reperfusion injury in rats. Stem cells international. 2018;2018:1-7.

https://doi.org/10.1155/2018/4659159

59. Tsai MJ, Tsai SK, Hu BR, Liou DY, Huang SL, Huang MC, et al. Recovery of neurological function of ischemic stroke by application of conditioned medium of bone marrow mesenchymal stem cells derived from normal and cerebral ischemia rats. Journal of biomedical science. 2014;21(1):1-12. http://www.jbiomedsci.com/content/21/1/5

60. Hicks C, Stevanato L, Stroemer RP, Tang E, Richardson S, Sinden JD. In Vivo and In Vitro Characterization of the Angiogenic Effect of CTX0E03 Human Neural Stem Cells. Cell Transplant. 2013;22:1541–52.

Figures

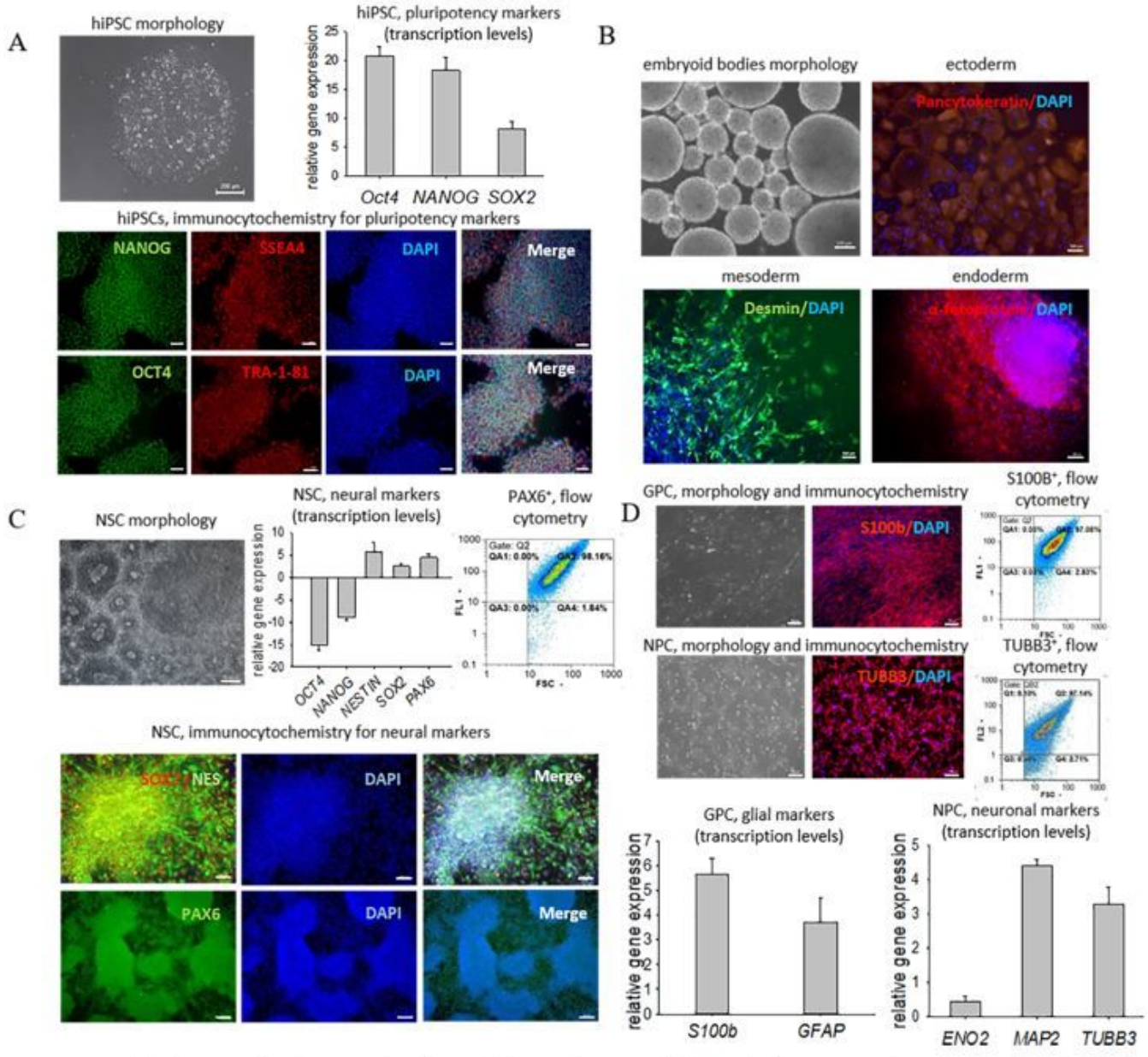

Figure 1

Morphology and characterization of the cultures differentiating towards neuronal and glial phenotypes. A Characterization of hiPSCs: phase-contrast microscopy, immunocytochemistry for the pluripotency markers (SSEA4, TRA-1-81, OCT4, NANOG), relative gene expression levels for OCT4, SOX2 and NANOG. B Functional assay of pluripotency: phase-contrast microscopy of the embryoid bodies and immunocytochemistry of spontaneously differentiated hiPSC derivatives with ectoderm-, mesoderm- and endoderm-specific antibodies (respectively, pan-cytokeratin, desmin and α-fetoprotein). C Characterization of NSCs: phase-contrast microscopy, immunocytochemistry and relative gene expression levels for neural markers (PAX6, NES, SOX2), flow cytometry for PAX6+ cells. D Characterization of GPCs and NPCs: phase-contrast microscopy, immunocytochemistry for S100B (glial marker) and βIII tubulin (TUBB3, neuronal marker), flow cytometry for S100B+ and TUBB3+ cells, relative gene expression levels for glial and neuronal markers.

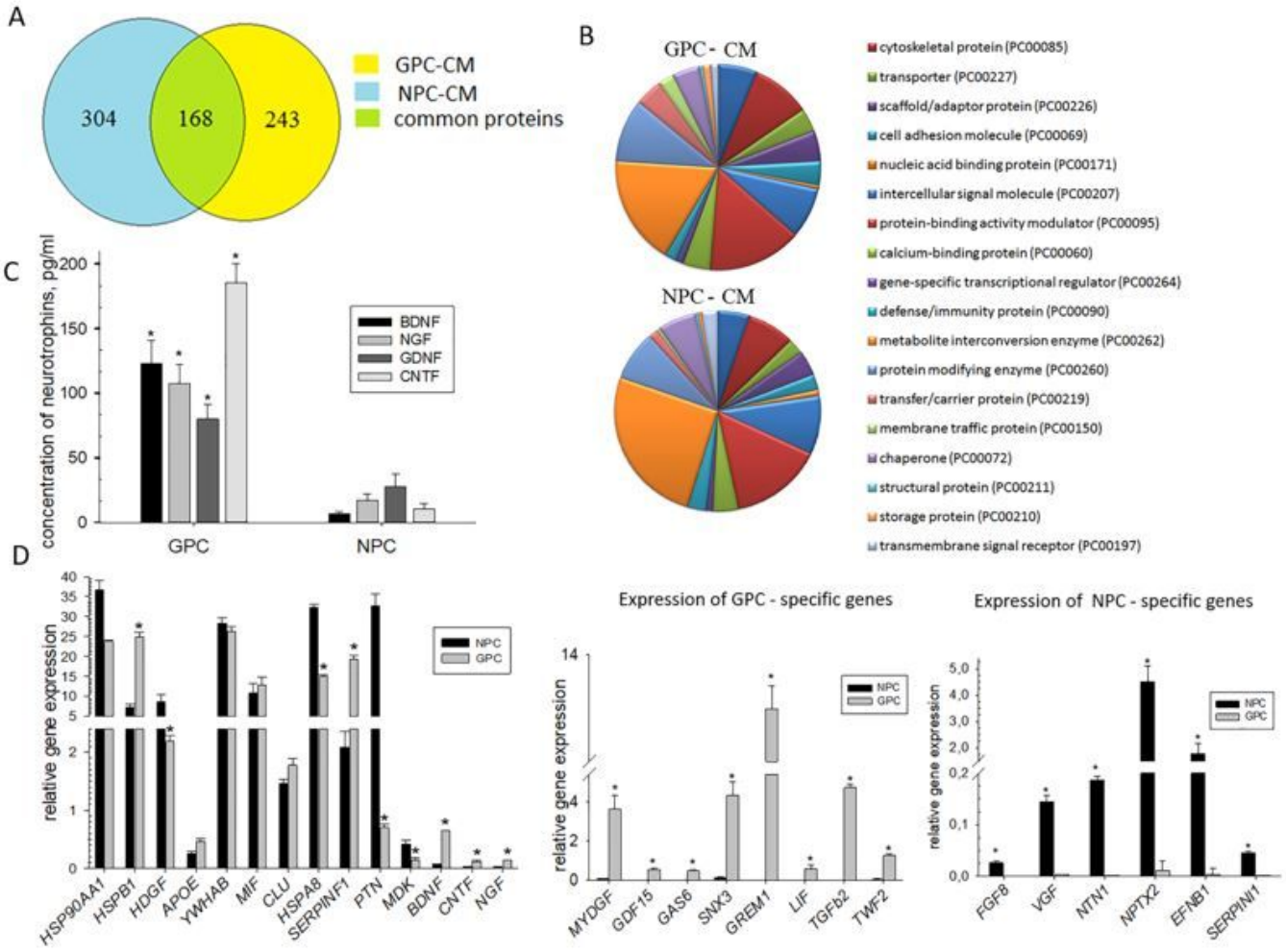

Figure 2

Comparative analysis of secretory activity and transcription profiles of the hiPSC-derived NPC and GPC cultures. A Proportions of unique and common proteins in NPC and GPC secretomes. B PANTHER protein class charts for NPC and GPC secretomes. C Secretion of neurotrophins by NPC and GPC (ELISA). D

Expression levels of NPC and GPC markers (PCR assay). The data are presented as mean□SD. Asterisks (*) indicate significant differences ($p \leq 0.05$).

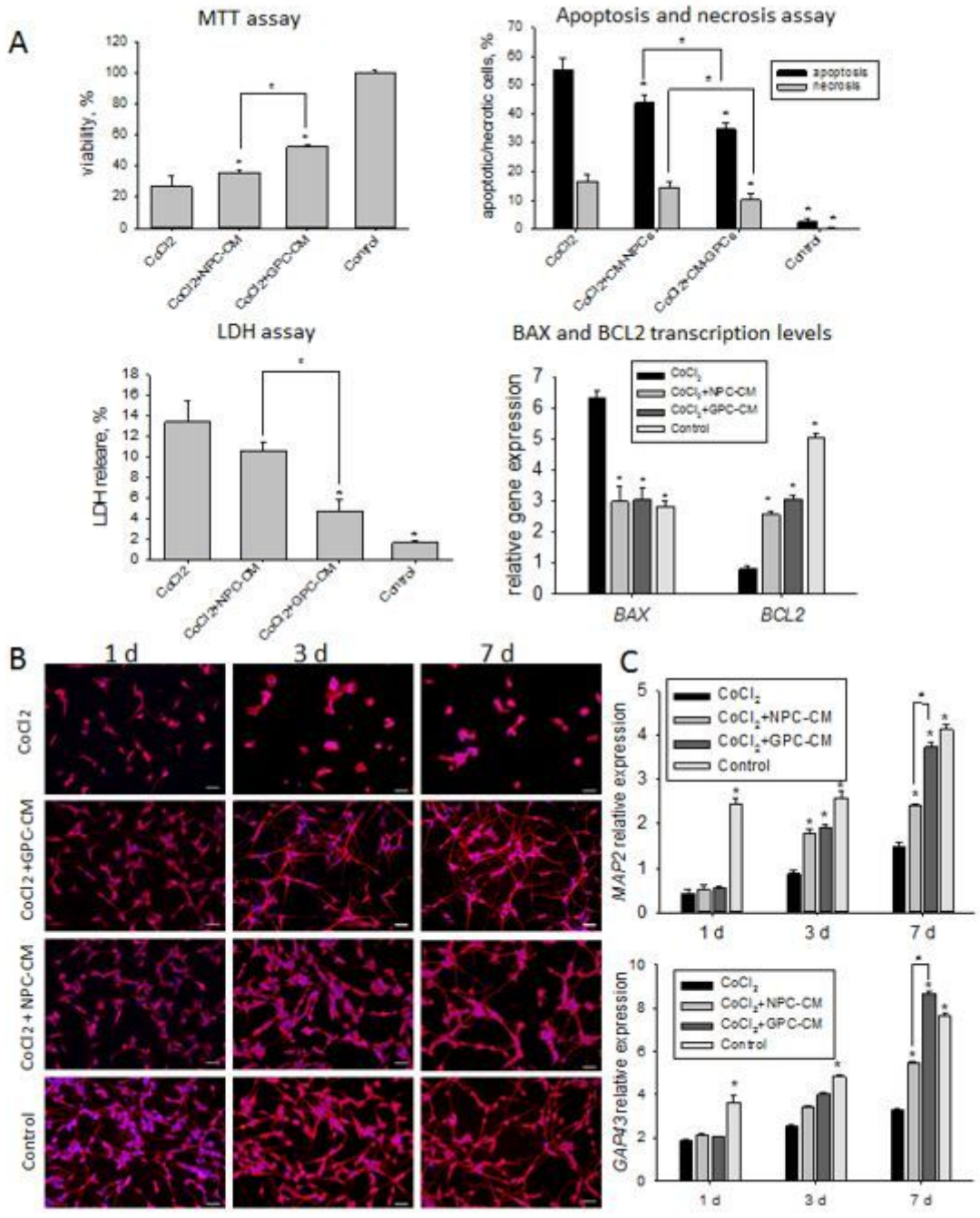

Figure 3

Neuroprotective effects of NPC-CM and GPC-CM in the in vitro hypoxia model. A Evaluation of the SHSY-5Y cell viability by MTT test, LDH test (levels of LDH released by necrotic cells), relative counts of apoptotic and necrotic cells, and BAX and BCL2 gene expression levels. B Immunocytochemical staining of SH-SY5Y cells with anti-βIII tubulin antibodies (nuclei counterstained with DAPI, blue). Scale bar, 100 μm. C Relative gene expression levels of MAP2 and GAP43. The data are presented as mean□SD.

Asterisks (*) indicate significant differences (p≤0.05) with the CoCl2 treated cultures. Hashes (#) indicate significant differences (p≤0.05) between GPC-CM and NPC-CM treated cultures.

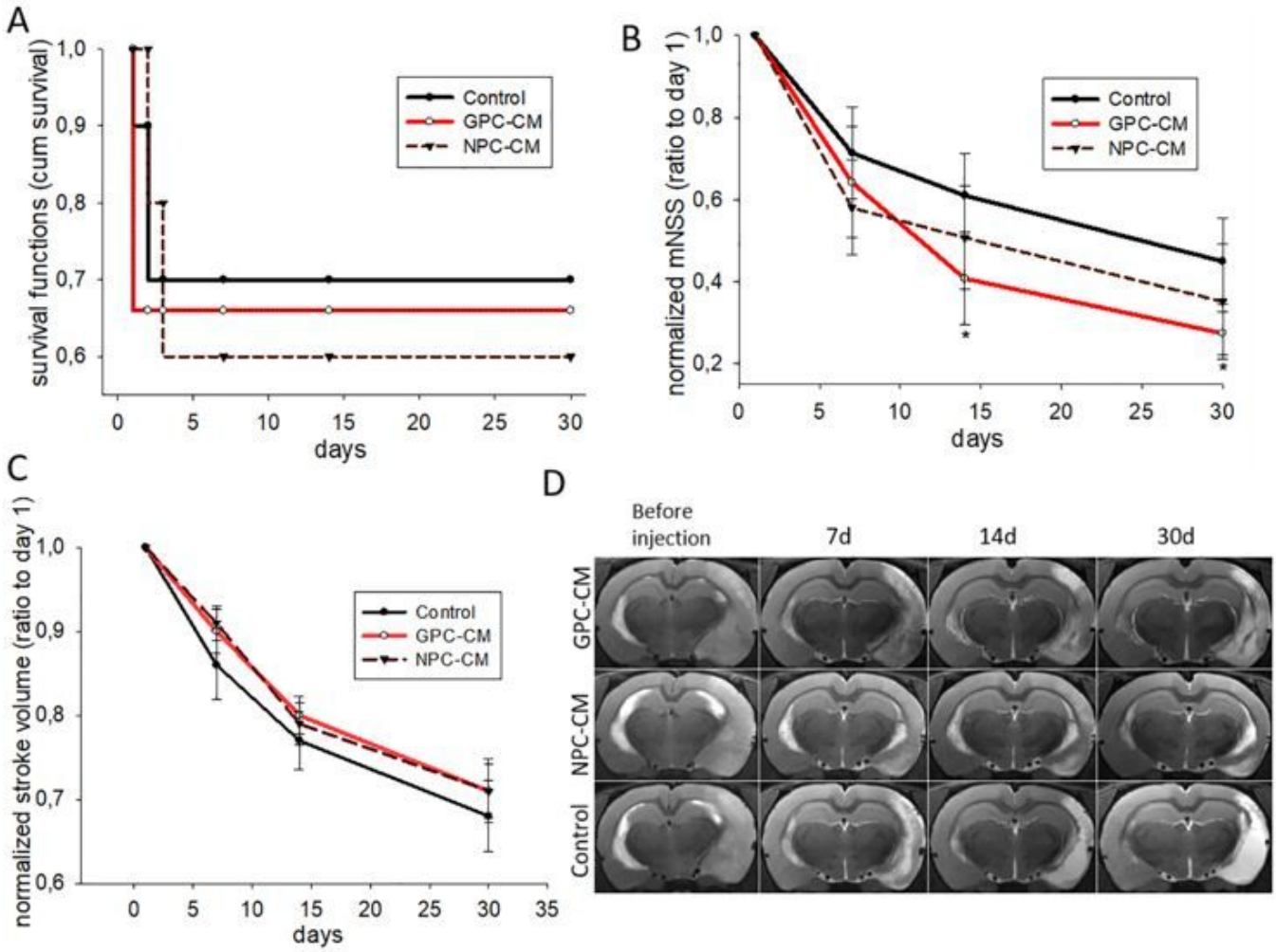

Figure 4

Therapeutic effects of NPC-CM and GPC-CM assessed by overall survival, dynamics of the stroke volume (evaluated by MRI) and dynamics of the neurological deficit (evaluated by mNSS for rodents). A Kaplan-Meier survival curves for three groups (NPC-CM treated, GPC-CM treated and the non-conditioned media-treated control). B mNSS dynamics (normalized by day 1 values). C infarct volume dynamics (normalized by day 1 values). D T2-weighted brain images (T2-WI) for three groups (NPC-CM treated, GPC-CM treated and the non-conditioned media-treated control). The data are presented as mean□SD with asterisks (*) indicating significant differences in comparison with the control (p ≤ 0.05).

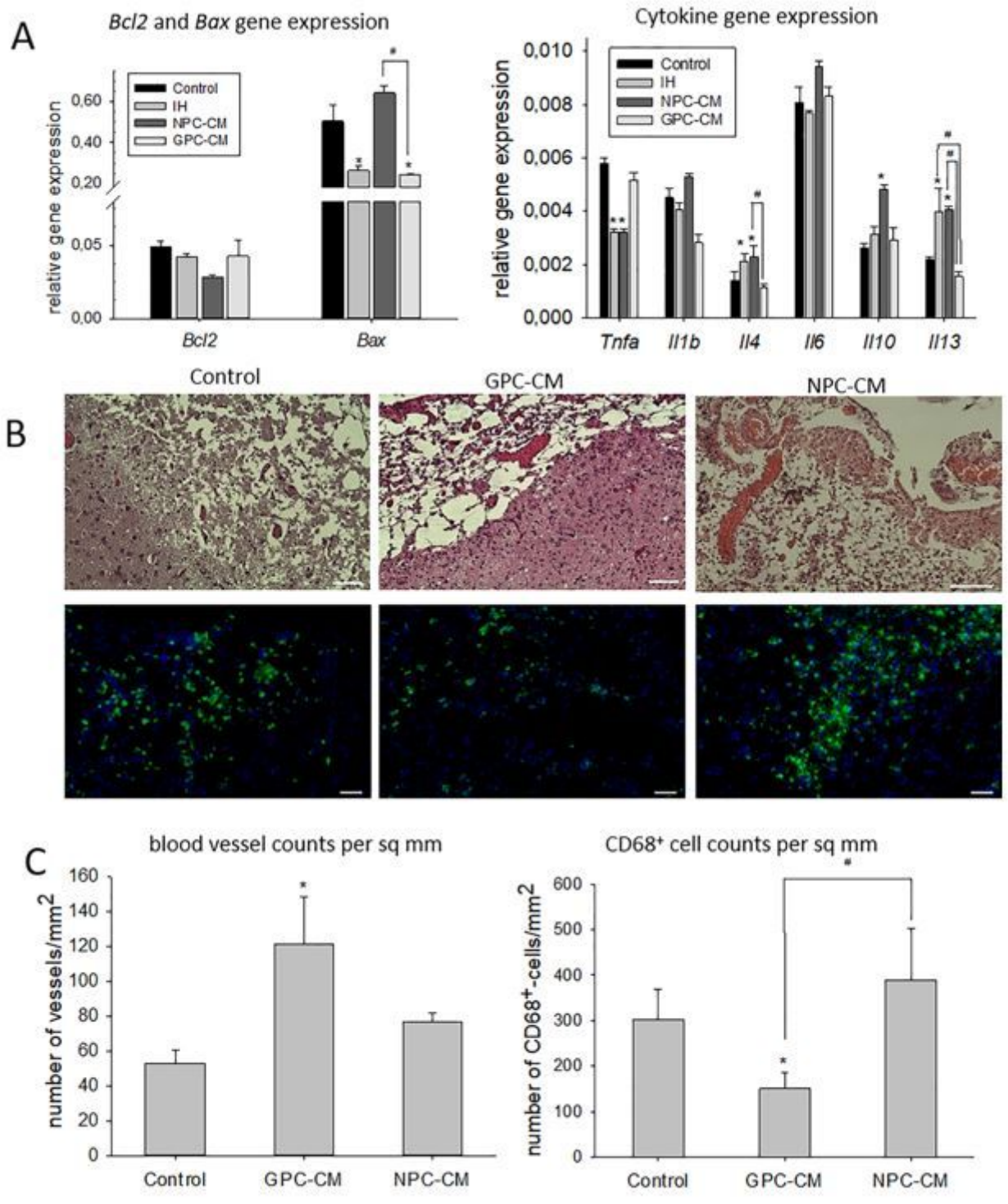

Figure 5

Post-ischemic repair- and inflammation-related effects of the conditioned media. A Relative expression levels of Bax and Bcl2; relative gene expression levels for pro- and anti-inflammatory cytokines. B Representative routine histology images (H&E) and immunohistochemistry with anti-CD68 antibodies (the nuclei counterstained with DAPI). Scale bar, 100 μm. C Counts of blood vessels and CD68+ cells per sq mm of the brain tissue section area. The data are presented as mean□SD. Asterisks (*) indicate significant

differences ($p \leq 0.05$) with the controls. Hashes (#) indicate significant differences ($p \leq 0.05$) between GPC-CM and NPC-CM treated animals.

Supplementary Files

This is a list of supplementary files associated with this preprint. Click to download.

- proteomicanalysis.xlsx
- SupplementaryTable.docx